Double-sided structural color of Fe_3O_4@SiO_2 nanoparticles under the electric field

Jianfei Zhang [a, b], Chengyi Chu [a], Aihua Sun [a, *], Si Ma [a], Xuanxuan Qiao [a], Chongyang Wang [a, b], Jianjun Guo [a], Zhixiang Li [a], Gaojie Xu [a]

[a] Ningbo Institute of Material Technology and Engineering, Chinese Academy of Sciences, & Key Laboratory of Additive Manufacturing Materials of Zhejiang Province, Ningbo 315201, PR China
[b] Department of Physics, Faculty of Science, Ningbo University, Ningbo 315211, PR China

ARTICLE INFO

Keywords:
Nanoparticles
Suspensions
Structural color
Core-shell
Fe_3O_4

ABSTRACT

The double-sided structural color of Fe_3O_4@SiO_2 NPs under external electric field was found. Corresponding colloidal suspension of Fe_3O_4@SiO_2 showed a highly adjustable structure color change on both sides of the display cell with the applying of electric fields. As the applied voltage increased, the color changed from red to green then to blue at positive plate, at the same time, the color changed from red to gray then to red at the negative plate. Under a certain electric field, the reflection peak move backwards within a particular range of wavelength. It may be caused by the emergence of another repulsive force-"solvation force" at small interparticle distances.

1. Introduction

Structural colors in nature, such as those on butterfly wings, beetle cuticles and peacock feathers, have attracted considerable attention in a variety of research areas [1–6]. Structural colors play major roles in natural and have a broad range of applications in color display, paint, cosmetics, and other many devices that require active optical components [7,8]. The color is due to light interference, diffraction, and scattering on internal with nano or microstructures composed of different refractive index materials that are comparable to the visible wavelength of light. The interaction of light with materials' periodic structure resulted in structural color, the color can be tuned by modulating the periodicity or refractive index of materials. By altering the periodicity of the photonic crystals, either through electrical, chemical, thermal or mechanical means, an induced swelling or contraction of the substrate will result in a shift in the wavelengths of light reflected and thus a change in color [9]. Colloidal suspensions are ideal candidates for making structurally colored materials, as they are inexpensive and also they can be dynamically manipulated with external fields [4–8]. Magnetic and electric fields are considered to be the optimal stimuli for modulation of the lattice constants of colloidal crystals for practical applications. Stabilized by the balance of attractive (magnetic) and repulsive (electrostatic) forces, colloids form ordered structures along the direction of the external field with regular interparticle spacing on the order of hundreds of nanometers [10]. Ge et al. [6] reported the magnetically tunable colloidal photonic structures in alkanol solutions of Fe_3O_4@SiO_2 colloidal structures. However, the magnetic field is often hard to be controlled precisely without interference the each other [11]. For electric field, the disadvantage of the magnetic field avoided. Using electric field as a stimulus source received increasing attention. For example, various colloidal particles such as Fe_3O_4@SiO_2, ZnS@SiO_2, and SiO_2@TiO_2 etc. have been used for the fabrication of photonic crystals with tuning the structural colors in response to the applied electric field [12–14]. While previous studies have linked the structural colors at the front of the display cell under the external field, few have focused on the back of the cell or compared the differences of structural colors between the both sides. In this paper, we found that the double sided display device showed different structural colors on each side of a surface by applying external electric field. This finding should provide new insights into the

* Corresponding author.
E-mail addresses: sunaihua@nimte.ac.cn (A. Sun), jjguo@nimte.ac.cn (J. Guo).

design and preparation of double sided display device.

In this article, three kinds of Fe_3O_4@SiO_2 core-shell particles with different diameters: a) core 100 nm, shell 25 nm, b) core 120 nm, shell 15 nm, c) core 120 nm, shell 25 nm were prepared. Due to the high electrophoretic mobility in organic solvents and high optical contrast, Fe_3O_4@SiO_2 core-shell nanoparticles were the ideal candidate [4]. SiO_2 shell is a successful example of introducing a steric hindrance, which can improve the stability and tolerance of photonic crystals [14,15]. The double-sided structural color of different Fe_3O_4@SiO_2 NPs suspension under electric field was studied, when an electric field of about 1.4 v was applied, the reflection peak appeared a red shift. Then with an increase of voltage, the reflection peak blue shifted again.

2. Experimental section

2.1. Chemicals

Trisodium citrate dehydrate (AR), Iron (III) chloride hexahydrate ($FeCl_3 \cdot 6H_2O$, AR), Ethanol (AR) were purchased from Sinopharm Chemical Reagent Company (Shanghai, China). Propylene carbonate (PC, 99%), ammonium hydroxide solution ($NH_3 \cdot H_2O$, AR, 25% ~28%), tetraethyl orthosilicate (TEOS, AR), ethylene glycol (EG, 99%), sodium acetate anhydrous (99%) were purchased from Aladdin Chemicals (Shanghai, China). Indium tin oxide (ITO) coated glass with a resistivity of 7 Ω·cm purchased from Corning Corp. All chemicals were used as received without further purification. The water used in this work was deionized (DI) water form a Millipor-Q purification system (Millipore, USA) of resistivity 18.2 MΩ·cm.

2.2. Synthesis procedures

Synthesis of Fe_3O_4 NPs and Fe_3O_4@SiO_2 core-shell particles: The synthesis route of Fe_3O_4 was based on the hydrothermal method. The approach similar to previous study and the modification of experimental parameters adopted to prepare sphere-like nanoparticles (NPs) [16,17]. The SiO_2 shell was synthesized by the hydrolysis of TEOS under mild conditions in an alcohol–ammonia solution. This approach is similar to the ammonia-catalyzed Stöber method [18]. The SiO_2 shell on the Fe_3O_4 core through the hydrolysis of TEOS under alkaline condition and obtain different thickness of SiO_2 shell.

2.3. Device preparation

The photonic display cell was consisting of two transparent electrodes separated by 200 μm thick epoxy spacers. The Fe_3O_4@SiO_2 suspension (12.6 v% in propylene carbonate) was injected into the cell through conventional injection syringe.

2.4. Characterization

The morphology and size of Fe_3O_4@SiO_2 NPs were carried out with field-emission scanning electron microscopy (FE-SEM, HITACHI S-4800) and transmission electron microscope (FEI Tecnai G2 F20). The reflection spectra of Fe_3O_4@SiO_2 colloidal suspensions under the trigger of electric field were measured by an Ocean Optics HR 2000CG-UV-NIR spectrometer coupled with a six-around-one reflection/back scattering probe. The electric field applied to Fe_3O_4@SiO_2 colloidal suspensions was adjusted a function generator (Agilent, 33220A) for the DC power supply. The ITO glasses were separated by Teflon with the thickness of 200 μm composed the sample cell (Diameter of 20 mm).

3. Results and discussion

SEM images of Fe_3O_4@SiO_2 core-shell particles are shown in Fig. 1. It can be seen that the Fe_3O_4@SiO_2 core-shell particles are spherical with an average diameter of about a) 150 nm, b) 150 nm, and c) 170 nm. The structure of Fe_3O_4@SiO_2 core-shell particles has been characterized by high resolution transmission electron microscopy (TEM) (Fig. 2). Obviously, the Fe_3O_4 together with a SiO_2 shell composed a core-shell structure a) core-100 nm, shell-25 nm ($C_{100}S_{25}$), b) core-120 nm, shell-15 nm ($C_{120}S_{15}$), c) core-120 nm, shell-25 nm ($C_{120}S_{25}$), respectively, which controlled the thickness of the shell through adjusting the amount of TEOS.

Fig. 3 shows the reflectance spectra of positive and negative plates of Fe_3O_4@SiO_2 with different sizes core-shell at concentrations of 12.6 v% in propylene carbonate under a varied electric potential, respectively. As seen from the reflection spectra of positive plates in Fig. 3(a, c, e), the reflection peak maximum value of Fe_3O_4@SiO_2 NPs increases gradually at first and then drops. The diffraction wavelength exhibits a similar tuning behavior along with the electric field strength variations. The reflection peaks at ~703 nm without the electrical potential at positive plate of Fe_3O_4@SiO_2 (core-100 nm, shell-25 nm) was observed in Fig. 3a. With the increase of the applied positive voltage to 2.0 v, the reflection peak position moved to ~493 nm due to the blue shift. Fig. 3c shows the reflectance spectra of positive plates of Fe_3O_4@SiO_2 (core-120 nm, shell-15 nm). Compared with the results of Fig. 3a, the range of the blue-shift was similar. With the increase of the applied positive voltage to 2.0 v, the reflection peak position shifted from ~711 nm to ~528 nm. Fig. 3e shows the reflectance spectra of positive plates of Fe_3O_4@SiO_2 (core-120 nm, shell-25 nm). The range of the blue-shift broader shifted from ~760 nm to ~538 nm than Fig. 3a, c. Due to the different thickness of shell, the effective refractive index of particles changed. The refractive index of Fe_3O_4 is 3.0 as SiO_2 is 1.6. The thin SiO_2 shell of particles had large effective refractive index at the same diameter. According to the Bragg diffraction formula [19].

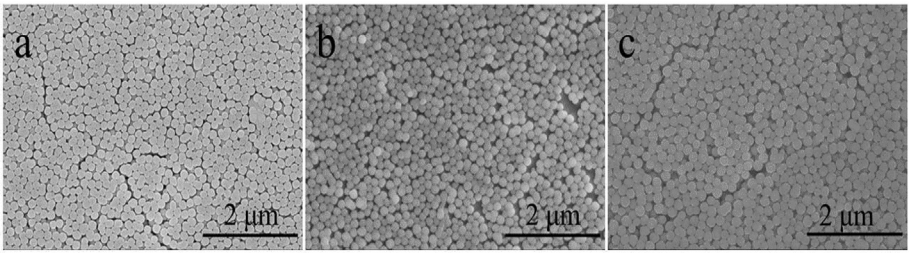

Fig. 1. SEM images of different diameters of Fe_3O_4@SiO_2 core-shell particles a) core 100 nm, shell 25 nm, b) core 120 nm, shell 15 nm, c) core 120 nm, shell 25 nm.

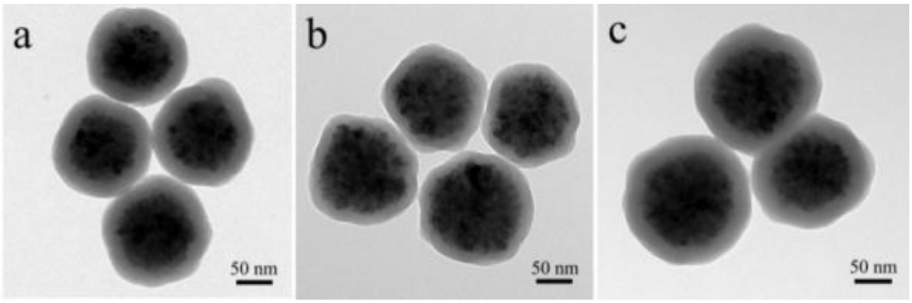

Fig. 2. TEM images of different diameters of Fe_3O_4@SiO_2 core-shell particles a) core 100 nm, shell 25 nm, b) core 120 nm, shell 15 nm, c) core 120 nm, shell 25 nm.

$$\lambda = 2dn_{eff} = \left(\frac{\pi}{3\sqrt{2}\varphi}\right)^{1/3}\left(\frac{8}{3}\right)^{1/2} D\left(n_p^2\varphi + n_m^2(1-\varphi)\right)^{1/2}$$

(where λ is the diffraction wavelength, d is the interparticle distances, n_{eff} is the effective refractive index, D is the diameter of particles, φ is the volume fraction of particles, n_p is the refractive index of particles, n_m is the refractive index of medium.) The diffraction wavelength of $C_{120}S_{15}$ was larger than $C_{100}S_{25}$ because of the large effective refractive index. Due to the size of the Fe_3O_4@-SiO_2 particles in Fig. 3e is larger than Fig. 3a and c. Because of the larger size of particles, the interparticle distance was broader at the

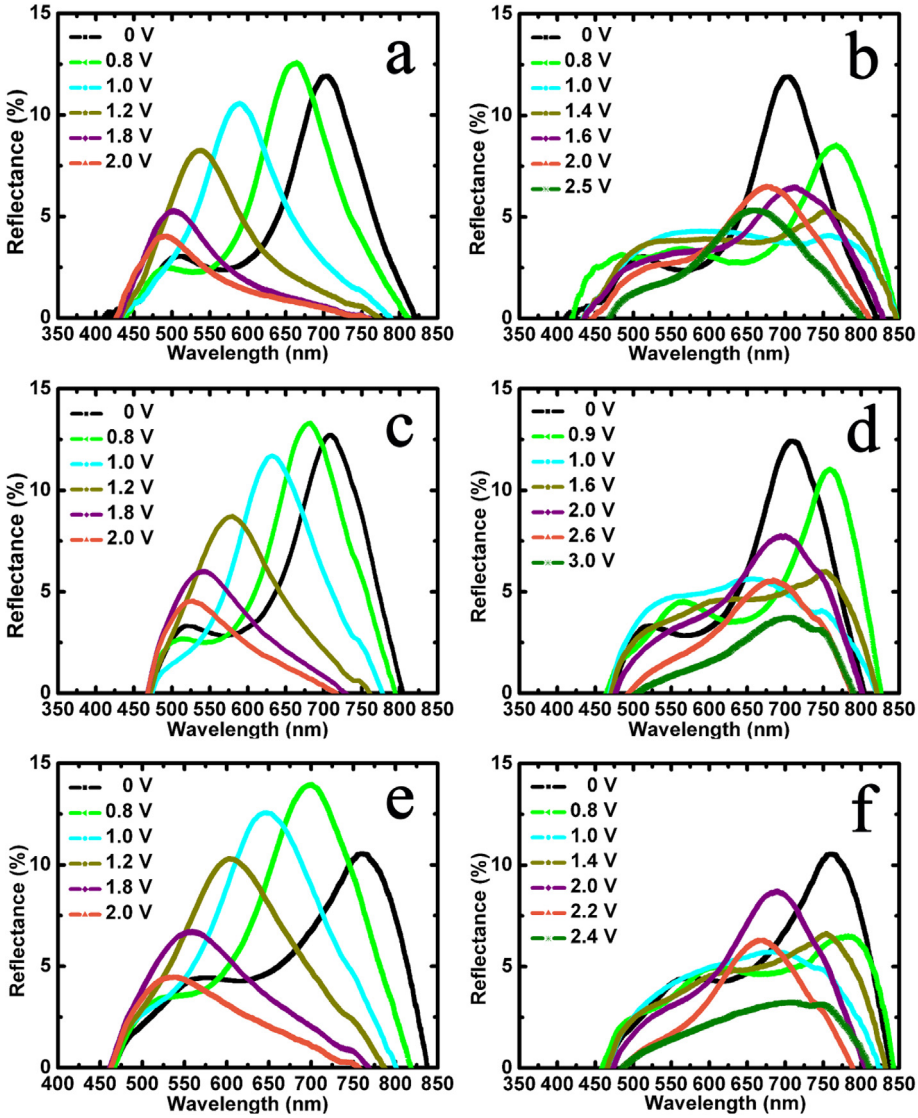

Fig. 3. Reflection spectra of positive and negative plates of Fe_3O_4@SiO_2 colloidal suspensions with different sizes of core-shell under different positive bias voltage. a) $C_{100}S_{25}$ positive plate b) $C_{100}S_{25}$ negative plate c) $C_{120}S_{15}$ positive plate d) $C_{120}S_{15}$ negative plate e) $C_{120}S_{25}$ positive plate f) $C_{120}S_{25}$ negative plate.

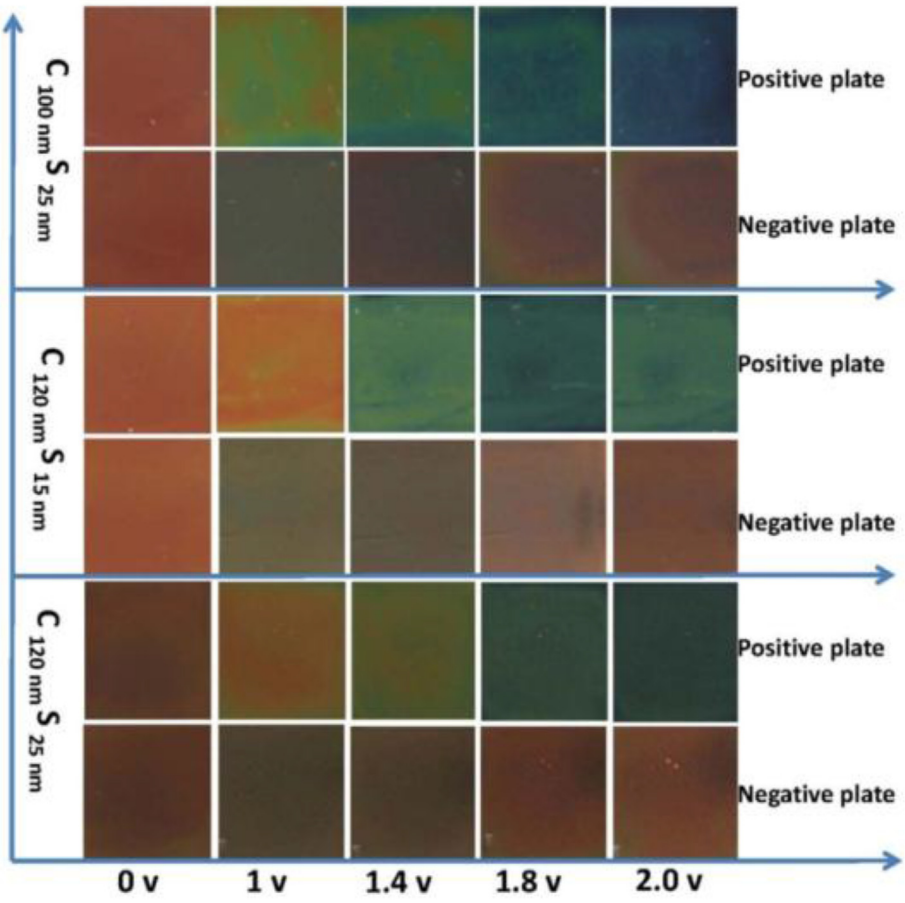

Fig. 4. The photos of positive and negative plate of Fe_3O_4@SiO_2 colloidal suspensions with different sizes of core or shell under different positive bias voltage.

same electric field according to the Bragg equation. As a result the reflection spectra red shifted entirely.

From the reflection spectra of negative plates of Fe_3O_4@SiO_2 in Fig. 3(b, d, f), it can be seen that the diffraction wavelength exhibits a similar tuning behavior along with the electric field strength variations. The reflection peak first red shifted and the intensity decreased quickly, when an electric field about of 1.0 v was applied, the reflection peak began a blue shifted in red spectral region in Fig. 3b. Compared with the results of Fig. 3b, the reflection spectra changed similarly in Fig. 3d and f except the different voltage of blue shift.

The corresponding photographs taken at 0 v, 1.0 v, 1.4 v, 1.8 v, 2.0 v of Fe_3O_4@SiO_2 with different sizes of the core or shell were showed in Fig. 4 at concentrations of 12.6 v% in propylene carbonate. The change of color was obvious at positive plate. As the applied voltage increased, the color changed from red to green and blue. At the negative plate the change of color was also observed obviously. Due to interparticle distance was increased, the color changed to gray at about 1.0 v. Interparticle distance decreased relatively as further increased voltage, the color displayed red. On account of the amount of Fe_3O_4@SiO_2 particles, the distance was not nearly enough to display other colors.

Fig. 5 shows the schematic representation of the double-sided structural color of Fe_3O_4@SiO_2 nanoparticles under the electric field. The Fe_3O_4@SiO_2 particles dispersed homogeneously in propylene carbonate without electrical potential at the positive plate. With the increase of the applied positive voltage, the particles moved to the positive plate. The particles arranged in orderly structures under the electric field force and the interparticle force. The key of structural color tuning is the interparticle distance. With the increase of the applied positive voltage the interparticle distance of the Fe_3O_4@SiO_2 decreased. As the distance decrease, the blue-shift of the reflection peak occurred. For the negative plate due to the concentration of the Fe_3O_4@SiO_2 suspension, the position of reflection peak at ~703 nm. (Fig. 3b) With the increase of the applied positive voltage, the amount of particles on the negative plate decreased due to electrophoresis. The reflection peak first red shifted due to the increased interparticle distance. Although the

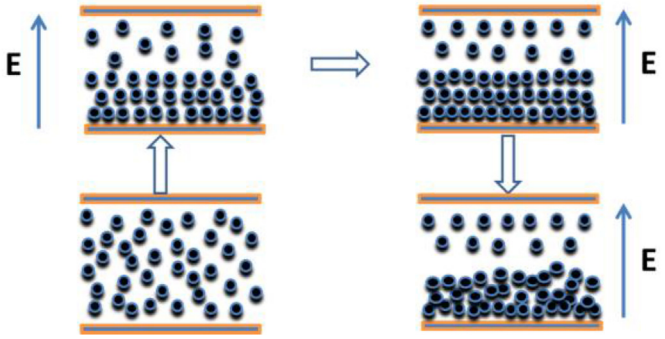

Fig. 5. Schematic representation of the double-sided structural color of Fe_3O_4@SiO_2 nanoparticles under the electric field. (For interpretation of the references to colour in this figure legend, the reader is referred to the web version of this article.)

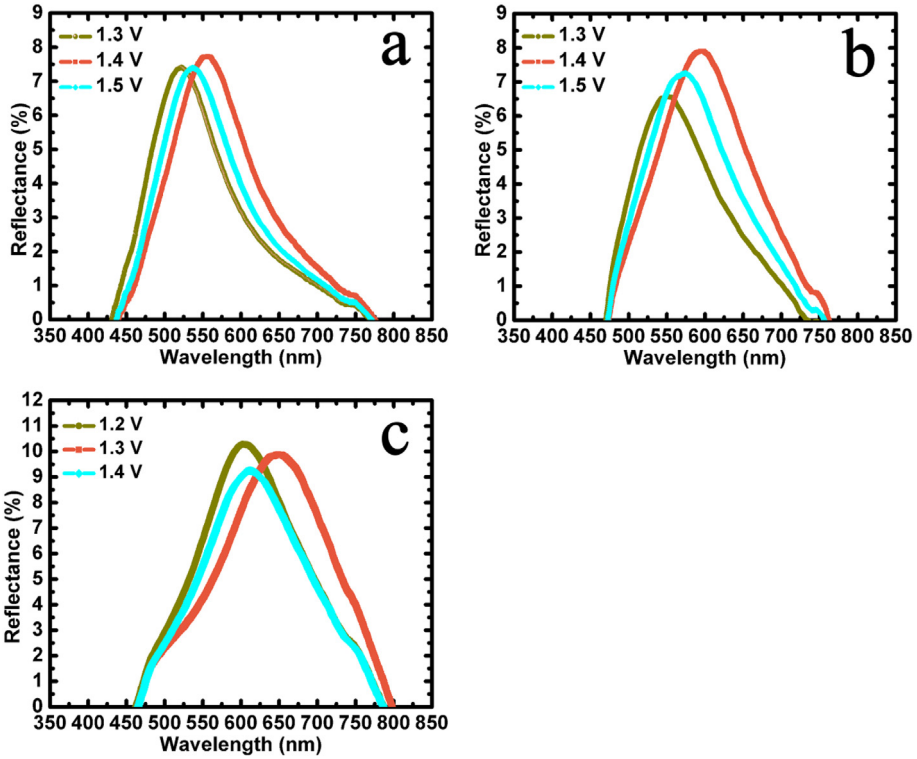

Fig. 6. The red shift reflection spectra of positive plates of Fe_3O_4@SiO_2 colloidal suspensions under different positive bias voltage. a) $C_{100}S_{25}$ positive plate b) $C_{120}S_{15}$ positive plate c) $C_{120}S_{25}$ positive plate. (For interpretation of the references to colour in this figure legend, the reader is referred to the web version of this article.)

amount of particles decreased, the interparticle distance decreased when the applied voltage large enough. Also the particles arranged in orderly structures under the electric field force and the interparticle force on the negative plate. The reflection peak blue shifted in red regional on account of the large interparticle distance with the increase of the applied positive voltage.

Overall, the reflection peak blue shift and the intensity decreased at the positive plate. From Fig. 6 it can be seen that the reflection peak appeared a red shift then blue shift again with the increase of voltage. When an electric field of about 1.4 v was applied, the reflection peak appeared a red shift. With the increase of voltage, the reflection peak blue shifted again. Table 1 shows the reflection peak position under the applied positive voltage at positive plate. From Table 1 the position of reflection peak at ~522 nm at 1.3 v for $C_{100}S_{25}$. After a positive voltage of 1.4 v was applied, the reflection peak red shift to ~556 nm. The reflection peak blue shifted to 522 nm, when the voltage increased to 1.6 v. Compared with the results of $C_{100}S_{25}$, the reflection spectra of $C_{120}S_{15}$ and $C_{120}S_{25}$ changed similar to $C_{100}S_{25}$. The distinction of $C_{120}S_{25}$ was the different voltage of red shift at 1.3 v.

The schematic representation of the stress analysis of Fe_3O_4@-SiO_2 nanoparticles under the electric field was showed in Fig. 7. In the large distance, the particles reached a state of equilibrium and arranged into a short-range ordered structures under the electrostatic force, electric field force, gravity, dipole and resistance rooting to the solvation. With the increase of the electric field, the diffraction peak blue shifted and the interparticle distances decreased. In the process, gravity and resistance rooting to the solvation remained unchanged while the electrostatic force and electric field force increased. The dipole had little change due to the weak interaction between particles. The particles will be closed to each other on account of the increased rapidly electric field force comprised with electrostatic force. When the interparticle distance was small enough, in addition to the relatively long-range electrostatic interactions, another repulsive force-"solvation force"- appeared [20–22]. We considered that the new repulsive force-"solvation force"- is the main reason of the red shift. The particles reached a new state of equilibrium and arranged into a short-range ordered structures. The reflection peak appeared a red shift on account of the increased interparticle distances due to the appeared solvation force. The solvation force comes from the overlap of two solvation layers on the particle surface. A disjoining pressure develops and eventually prevents them from coming even closer when particles approach each other [21–23]. Solvation forces

Table 1
The position of reflection peak under the applied positive voltage at the positive plate.

Samples	1.1 v	1.3 v	1.4 v	1.6 v	1.8 v
$C_{100}S_{25}$	537 nm	522 nm	556 nm	522 nm	500 nm
$C_{120}S_{15}$	598 nm	550 nm	597 nm	556 nm	540 nm
$C_{120}S_{25}$	624 nm	648 nm	612 nm	585 nm	559 nm

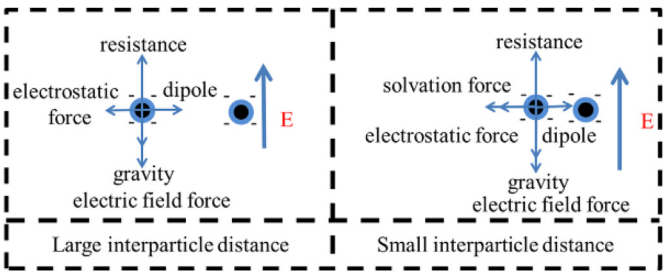

Fig. 7. Schematic representation of the stress analysis of Fe_3O_4@SiO_2 nanoparticles under the electric field.

depend both on the chemical and physical properties of the surfaces being considered, such as the wettability, surface morphology, crystal structure and rigidity and on the properties of the intervening medium [23]. Derjaguin and Churaev proposed that the solvation force between quartz particles in the water medium, which arise at a few nanometers separation distances [24,25]. A formula for determining the thickness of solvation films on solid particles in suspensions is presented on the basis of Einstein's theory of the viscosity of dispersions [22]. The solvation force appeared at dozens of nanometer due to the higher viscosity of propylene carbonate compared to water. According to the Bragg diffraction formula: $\lambda = 2dn_{eff}\sin\theta$. Where λ is the diffraction wavelength, d is the interparticle distances, n_{eff} is the effective refractive index. The interparticle distances which we can calculate the interparticle distances utilized the Bragg diffraction formula is very correspond to that Derjaguin and Churaev proposed. At the dozens of nanometer between the surfaces of particles, the solvation force will arise. The particles reached a new state of equilibrium under the electrostatic force, electric field force, gravity, dipole, resistance and solvation force. So the diffraction peak red shift at a specific voltage. With the increase of voltage, the reflection peak blue shifted again on account of the increase of the electric field force.

4. Conclusions

In summary, corresponding colloidal suspension of Fe_3O_4@SiO_2 showed a highly adjustable structure color change on both sides of the display cell with the applying of electric fields. The double-sided structural color of Fe_3O_4@SiO_2 NPs under external electric field was found. The particles on positive or negative plate arranged in an orderly structure under the effect of electric field force and static electricity. Under a certain electric field, the reflection peak move backwards within a particular range of wavelength. The tunable photonic structures formed in propylene carbonate solutions by assembling Fe_3O_4@SiO_2 core-shell particles using electric field. When an electric field of about 1.4 v was applied, the reflection peak appeared a red shift. With the increased of voltage, the reflection peak blue shifted again. This phenomenon depends on the electrostatic force, electric field force, gravity, dipole, resistance and solvation force.

Acknowledgment

This project is supported by National Natural Science Foundation of China (Grant no. 11374311, 11404347), the Ningbo Natural Science Foundation (2012A610121, 2014A610123).We also express our gratitude to the aided program for Science and Technology Innovative Research Team of Ningbo Municipality (2015B11002).

References

[1] A.C. Arsenault, D.P. Puzzo, I. Manners, G.A. Ozin, Nat. Photonics 140 (2007) 468.
[2] D.P. Puzzo, A.C. Arsenault, I. Manners, G.A. Ozin, Angew. Chem. Int. Ed. l48 (2009) 943.
[3] X.L. Xu, G. Friedman, K.D. Humfeld, S.A. Majetich, S.A. Asher, Adv. Mater 13 (2001) 1681.
[4] I. Lee, D. Kim, J. Kal, H. Baek, D. Kwak, D. Go, E. Kim, C. Kang, J. Chung, Y. Jang, S. Ji, J. Joo, Y. Kang, Adv. Mater 22 (2010) 4973.
[5] J.P. Ge, Y.D. Yin, Angew. Chem. Int. Ed. 50 (2011) 1492.
[6] J.P. Ge, Y.G. Hu, Y.D. Yin, Angew. Chem. 119 (2007) 7572.
[7] S. Ekaterina, H. Christer, H.J. Daniel, K. Jostein, PNAS 108 (2011) 2668.
[8] B.R. Wasik, S.F. Liew, D.A. Lilienb, A.J. Dinwiddiea, H. Noh, H. Cao, A. Monteiro, PNAS 111 (2014) 12109.
[9] J. Xu, Z. Guo, J. Colloid Interface Sci. 406 (2013) 1.
[10] S.L. Pu, M. L, J. Alloys Compd. 481 (2009) 851.
[11] Y.G. Hu, L. He, X.G. Han, M.S. Wang, Y.D. Yin, Nano Res. 8 (2015) 611.
[12] Y.X. Luo, J.F. Zhang, A.H. Sun, C.Y. Chu, S. Zhou, J.J. Guo, G.J. Xu, J. Mater. Chem. C 2 (2014) 1990.
[13] M.G. Han, C.G. Shin, S.J. Jeon, H.S. Shim, C.J. Heo, H.S. Jin, J.W. Kim, S.Y. Lee, Adv. Mater 24 (2012) 6438.
[14] J.P. Ge, H. Lee, L. He, J. Kim, Z.D. Lu, H. Kim, J. Goebl, S. Kwonand, Y.D. Yin, J. Am. Chem. Soc. 131 (2009) 15687.
[15] X.X. Qiao, Y.X. Luo, A.H. Sun, C.Y. Wang, J.F. Zhang, C.Y. Chu, J.J. Guo, G.J. Xu, RSC Adv. 5 (2015) 6489.
[16] J.F. Zhang, X.X. Qiao, A.H. Sun, C.Y. Chu, C.Y. Wang, T. Chen, J.J. Guo, G.J. Xu, Mater. Res. Express 1 (2014) 045037.
[17] H. Deng, X.L. Li, Q. Peng, X. Wang, J.P. Chen, Y.D. Li, Angew. Chem. 117 (2005) 2842.
[18] W. Stober, A. Fink, E. Bohn, J. Colloid Interface Sci. 26 (1968) 62.
[19] T.S. Shim, S.H. Kim, J.Y. Sim, J.M. Lim, S.M. Yang, Adv. Mater 22 (2010) 4494.
[20] J.P. Ge, Y.D. Yin, J. Mater. Chem. 18 (2008) 5041.
[21] J. Ren, S. Song, A. Lopez-Valdivieso, J. Shen, S.J. Lu, Colloid Interface Sci. 238 (2001) 279.
[22] S. Song, C. Peng, J. Dispers. Sci. Technol. 26 (2005) 197.
[23] Y. Liang, N. Hilal, P. Langston, V. Starov, Adv. Colloid Interface Sci. 151 (2007) 134.
[24] B.V. Derjaguin, N.V. Churaev, J. Colloid Interface Sci. 49 (1974) 249.
[25] N.V. Churaev, B.V. Derjaguin, J. Colloid Interface Sci. 103 (1985) 542.